ISSN 0915-633X

NATIONAL INSTITUTE FOR FUSION SCIENCE

Simplified ν_μ , $\bar{\nu}_\mu$ Beam Detector and ν_μ, $\bar{\nu}_\mu$ Beam Source by Interaction between an Electron Bunch and a Positive Ion Bunch

J. Uramoto

(Received - Feb. 10, 1998)

NIFS-544 Mar. 1998

RESEARCH REPORT
NIFS Series

NAGOYA, JAPAN

Simplified ν_μ, $\bar{\nu}_\mu$ beam detector and ν_μ, $\bar{\nu}_\mu$ beam source by interaction between an electron bunch and a positive ion bunch

Jōshin URAMOTO

National Institute for Fusion Science,

Oroshi-cho, Toki-shi, Gifu, 509-5292, Japan

Abstract

Both positive pionlike (π^+) and negative pionlike (π^-) particles are created by interaction between an electron bunch and a positive ion bunch which are produced from a low energy (1 KeV) electron beam, a neutral gas and a perpendicular uniform magnetic field. These pionlike particles are shot into a thick metal plate MP. When positive ions (above a critical ion energy) are supplied in the opposite side of MP, some negative muonlike particles μ^- appear continuously. Similarly, when electrons (above a critical electron energy) are supplied in the opposite side of MP, some positive muonlike particles μ^+ appear continuously. From the thickness of MP, unknown particles penetrating MP are estimated to be μ neutrinos ν_μ and anti-μ neutrinos $\bar{\nu}_\mu$. These ν_μ and $\bar{\nu}_\mu$ sources are very simple as an experimental apparatus and can be developed much more in comparison with those from the H_2 gas discharge.

Keywords: negative muonlike particles μ^-, positive muonlike particles μ^+ μ neutrinos ν_μ and anti-μ neutrinos $\bar{\nu}_\mu$

We have reported[1),2)] already that positive or negative pions are extracted from outside of a H_2 gas discharge along magnetic field, and that μ-neutrino and anti-μ-neutrino beam are produced by shooting the positive or negative pion beam into a thick metal plate. In the outside of H_2 gas discharge, some high energy components of electron in a plasma are remained as the low energy components are lost by volume production of H^- ions. Moreover, the high energy electrons are accompanied with cyclotron motions due to the magnetic field. On the other hand, in the outside, positive ion beams generate when the outside boundary chamber potential is kept negatively in respect with the plasma potential (near the discharge anode). Thus, we can consider the high energy electrons and the positive ion beams as an origin of the pion generation under the H_2 gas discharge.

In this research, a secondary electron beam and positive ion beam which are produced by an electron beam and a gas, are injected perpendicularly to a uniform magnetic field in order to resolve mechanisms of the above pion generation, to develop the pion generation much more and to simplify the pion generation apparatus.

Schematic diagrams of the experimental apparatus are shown in Figs. 1. (It has been reported[3)] that both positive or negative pionlike particles are created in this experimental apparatus).

The distribution of electrically applied potential are shown in Fig. 2a. The first electron beam from the electron gun is perfectly reflected in front of the entrance slit S of the magnetic mass analyzer MA while a plasma is produced by a residual gas (air) ionization. Then, a positive ion beam is injected into MA through the slit S and the second electron beam is produced by reacceleration of the plasma electrons. It should be noted that the injected positive ion beam (i_2) is decelerated and stopped electrically, and that the second electron beam (e_2) suffers a magnetron (cyclotron) motion in the uniform magnetic field (which is used as the analyzing magnetic field of MA). As a result, both the electron beam and positive ion beam will be bunched within the small space at the entrance X of the uniform magnetic field.

Thus, we can expect a coherent interaction between the bunched electrons and positive ions.

Dependences of a positive or negative current $I^{\pm}$ to the beam collector BC on the analyzing magnetic field B_M or $-B_M$ are shown in Fig. 2b and 2c for a first electron beam acceleration voltage V_A of 1 kV. Here, we find that an analyzing relation of the positive or negative muon $\mu^{\pm}$ is

satisfied for the first peak of positive or negative current $I^{\pm}$, if we assume that the effective acceleration voltage V_E is twice of the first electron beam acceleration voltage V_A (which means the additional potential $+V = +V_A$ in Fig. 2a). That is, the following relation is found: From the analyzing magnetic field B_M where the positive or negative current shows a peak, the curvature radius r of the mass analyzer and the effective acceleration voltage V_E, we can estimate the mass m of the positively or negatively charged particle by,

$$m = \frac{Ze\,(B_M r)^2}{2V_E}$$

$$= \frac{8.8 \times 10^{-2}\, Z\,(B_M r)^2\, m_e}{V_E}, \quad \cdots\cdots (1)$$

where e is the electron charge, B_M is in gauss unit, r is in cm unit, V_E is in volt unit and m_e is the electron mass and Z is the charge number. For the curvature radius $r = 4.3$ cm of this mass analyzer, the Eq. (1) is rewritten by

$$m = \frac{1.63\, Z\, B_M^2}{V_E} m_e. \quad \cdots\cdots (2)$$

From Eq. (2) and the experimental conditions for the first peak of $I^{\pm}$ of Fig. 2b or 2c, we obtain $m = m_1 \approx 200\, m_e$ under $V_E = 2V_A = 2$ kV and $B_M \approx 510$ gauss, assuming that $Z = 1$. This experimental result means that positive or negative muonlike particles $\mu^{\pm}$ are produced (because the typical muon mass is near $207\, m_e$).

Moreover, we find the second peak of $I^{\pm}$ in Fig. 2b or 2c. From Eq. (2) and the experimental conditions, we obtain $m = m_2 \approx 285\, m_e$ under $V_E = 2$ kV and $B_M \approx 595$ gauss. This mass m_2 is near the typical pion mass ($273\, m_e$). That is, positive or negative pionlike particles $\pi^{\pm}$ are produced also. In the next experiment, the positive (π^+) or negative (π^-) pionlike particle beam is shot into a thick (~1 cm) metal plate MP as shown in Fig. 3a. Then, only a negative muonlike μ^- beam is observed in the positive side of MP while only positive ions can diffuse across the magnetic field (~500 gauss) behind MP from the secondary plasma (S.P. in Fig. 3a) which are produced around the analyzing magnetic field B_M or $(-B_M)$ by the injected ion beam I.B. and secondary

electron beam S.E.B.. In comparison with the cases[1),2)] of H_2 gas discharge, this experimental result of Fig. 3a shows that the pionlike particles $\pi^{\pm}$ agree with the true pions, and that μ-neutrino ν_μ and anti-μ-neutrino $\bar{\nu}_\mu$ beam penetrate the thick metal plate MP.

To confirm these facts furthermore, an external detector <Detector> for μ-neutrino ν_μ and anti-μ-neutrino $\bar{\nu}_\mu$ is arranged as shown in Fig. 3b which is above 50 cm away from the source <Source> as shown in Fig. 3a across two metal plates (BMP and DMP) and atmosphere. In the detector side, electron beams (e) or positive ion beams (i) are supplied between the metal plate DMP (receiving ν_μ and $\bar{\nu}_\mu$ beams) and the beam collector BC detecting positive or negative muon current (μ^+ or μ^-). The electron beams (e) or positive ion beams (i) are extracted from a discharge plasma between a cold cathode and an anode where a residual gas in the pressure of about 10^{-5} Torr is used, which can be selected by polarities of two extraction power supplies V_1 and V_2.

When the electron beams (e) in <Detector> are supplied, a positive muon current (μ^+) are observed as shown in Fig. 4a under both the analyzing magnetic field B_M and $-B_M$ in <Source>. Similarly, when the positive ion beams are supplied, a negative muon current (μ^-) is observed as shown in Fig. 4b. It should be noted that μ^+ and μ^- do not depend on the polarities of the analyzing magnetic field. These experimental results agree with the cases of the H_2 gas discharge in magnetic field which have reported[1),2)] already. However, this method from an electron beam and a residual gas is very advantageous as the experimental apparatus are simple and can be developed much more.

References

1) J. Uramoto: Research Report, NIFS– 541 (1998).

2) J. Uramoto: Research Report, NIFS– 542 (1998).

3) J. Uramoto: National Institute for Fusion Science, 332-6 Oroshi-cho, Toki-shi, Gifu, 509-52, Japan – Research Report, NIFS–529 (1997).

Figure Captions

Fig. 1**a** and **b** Schematic diagrams of the experimental apparatus.

F: Filament as electron emitter. K: Cathode of electron gun. A: Anode of electron gun. V_A: Initial electron acceleration voltage of 1 kV. I_A: Total negative current of 3 mA. F.E.B.: First electron beam. G: Neutral gas. D: Decelerator of F.E.B. S: Entrance slit (3 mm × 10 mm). Ins: Insulator. I.B.: Ion beam. S.E.B.: Second electron beam. e: Electrons with cyclotron motions. $\mu^{\pm}$: Positive or Negative muonlike particle. (MA): Mass analyzer. Fe: Iron. C: Magnetic Coil. (N): North pole of electro-magnet. (S): South pole. B_M: Analyzing magnetic field. BC: Beam collector. $I^{\pm}$: Positive and Negative current to BC. S.P.: Secondary plasma inside (MA). X: Entrance of uniform magnetic field. i: Ion bunch. $\pi^{\pm}$: Positive or Negative pionlike particle. Neutral gas pressure: 5×10^{-6} Torr.

c Fringe magnetic field distribution.

B_M: Analyzing magnetic field of (MA). B_O: Uniform magnetic field inside (MA). X: End of uniform magnetic field. S: Entrance slit position. Fe: Magnetic field distribution in a case using iron plate as D. Cu: Magnetic field distribution in a case using copper plate.

The initial or first electron beam (F.E.B.) is stopped critically in front of the entrance slit S by an electrical potential of the decelerator D connected to the cathode of the electron gun. Next, a neutral gas is introduced into the first electron beam region and a plasma is produced through ionization of the gas. Then, positive ions of the plasma are accelerated in front of S while a positive ion beam with an energy corresponding to the first electron beam acceleration voltage V_A, is injected into the magnetic field region through S. Moreover, the stopped beam electrons are reaccelerated electrically toward the gap between two magnetic poles (N) and (S) through S, while the injected ion beam is decelerated electrically and stopped in the gap. The electrically reaccelerated electrons are injected perpendicularly to the magnetic field (B_M) and bunched in cyclotron motions of small radius.

As shown in Fig. 1b, the above magnetic system is used as a mass analyzer (MA) of 90° type when the beam collector BC is arranged. The analyzing curvature radius r is 4.3

cm.

A magnetic field distribution of the analyzing magnetic field B_M under a magnetic coil current of 1A, is shown in Fig. 1c for two different metal plates as the entrance plate (decelerator D). In this apparatus, the iron (Fe) plate is used and the fringe magnetic field is much reduced.

Fig. 2 Applied electrical potential distribution.

a V: Electrical potential. V_A: Initial potential (voltage) of electron gun anode. V_E: Effective potential for $\mu^{\pm}$ (positive or negative muon) and $\pi^{\pm}$ (positive or negative pion). e_0: Initial electrons from electron gun cathode. e_1: First electron beam. e_2: Second electron beam. i_1: Positive ion beam from plasma. i_2: Second positive ion beam. e–B: Electron bunch due to magnetic cyclotron motion. i–B: Positive ion bunch due to electrical retardation. K: Cathode position of electron gun. A: Anode position of electron gun. S: Slit position of mass analyzer. X: Entrance position of analyzing uniform magnetic field. +V: Additional potential generated by stopping the positive ion beam.

b Dependence of the positive beam collector current I^+ on the analyzing magnetic field B_M under the initial electron acceleration voltage $V_A = 1$ kV and the total anode current $I_A = 3$ mA.

Neutral gas pressure is 1×10^{-5} Torr (Air) in the first electron beam region. μ^+: (means positive muonlike particle). π^+: (means positive pionlike particle).

c Dependence of the negative beam collector current I^- on the analyzing magnetic field $(-B_M)$ under the initial electron acceleration voltage $V_A = 1$ kV and the total anode current $I_A = 3$ mA.

Neutral gas pressure is 1×10^{-5} Torr (Air) in the first electron beam region. μ^-: (means negative muonlike particle). π^-: (means negative pionlike particle).

Fig. 3**a** Source of ν_μ and $\bar{\nu}_\mu$. The positive or negative pion $\pi^\pm$ beams are produced at the entrance (X) of uniform magnetic field B_M or $(-B_M)$ and are shot into a thick metal plate MP.

S.P.: Secondary plasma around the uniform magnetic field (mass analyzing magnetic field) B_M or $(-B_M)$ which are produced by injection of positive ion beam I.B. and secondary electron beam S.E.B.. BMP: Boundary metal plate. Others: see Figure captions of Figs. 1a and b. Neutral gas pressure: 5×10^{-6} Torr.

b Detector of ν_μ and $\bar{\nu}_\mu$. The ν_μ and $\bar{\nu}_\mu$ beams enter inside of <Detector> through the detector metal plate DMP.

BC: Beam collector of positive or negative muon (μ^+ or μ^-) beam which is caused by ν_μ or $\bar{\nu}_\mu$ and electron beam (e) or ion beam (i). A_d and K_d: Discharge anode and (cold) cathode. G: Residual gas (~10^{-5} Torr). V_d: Discharge voltage (≥ 400V). I_d: Discharge (dark) current (~20 μA). E_1 and E_2: Extraction electrodes with multi apertures. V_1: First extraction electrode power supply (~±30V). V_2: Second (final) extraction electrode ($|V_2| \geq 350$V), depends on first electron acceleration voltage V_A in Fig. 3a <Source>). e and i: Electron beams or positive ion beams which are produced from a very thin plasma by a discharge between A_d and K_d. Ins: Insulator for BC. $I_D^\pm$: Currents to BC.

Fig. 4 Characteristics of beam collector current $I_D^\pm$ at <Detector> in Fig. 3b.

a Dependence of the positive muon μ^+ current I_D^+ at <Detector> on the analyzing magnetic fields $\pm B_M$ of <Source> when the electron beams (e) are supplied at <Detector>. The initial electron acceleration voltage V_A = 1 kV and the total anode current I_A = 3 mA. Natural gas pressures are 1×10^{-5} Torr at <Detector> and 5×10^{-6} Torr at <Source>. V_1 = 30V. V_2 = 350V.

b Dependence of the negative muon μ^- current I_D^- at <Detector> on the analyzing magnetic fields $\pm B_M$ of <Source> when the positive ion beams (i) are supplied at <Detector>. V_1 = –30V. V_2 = –350V.

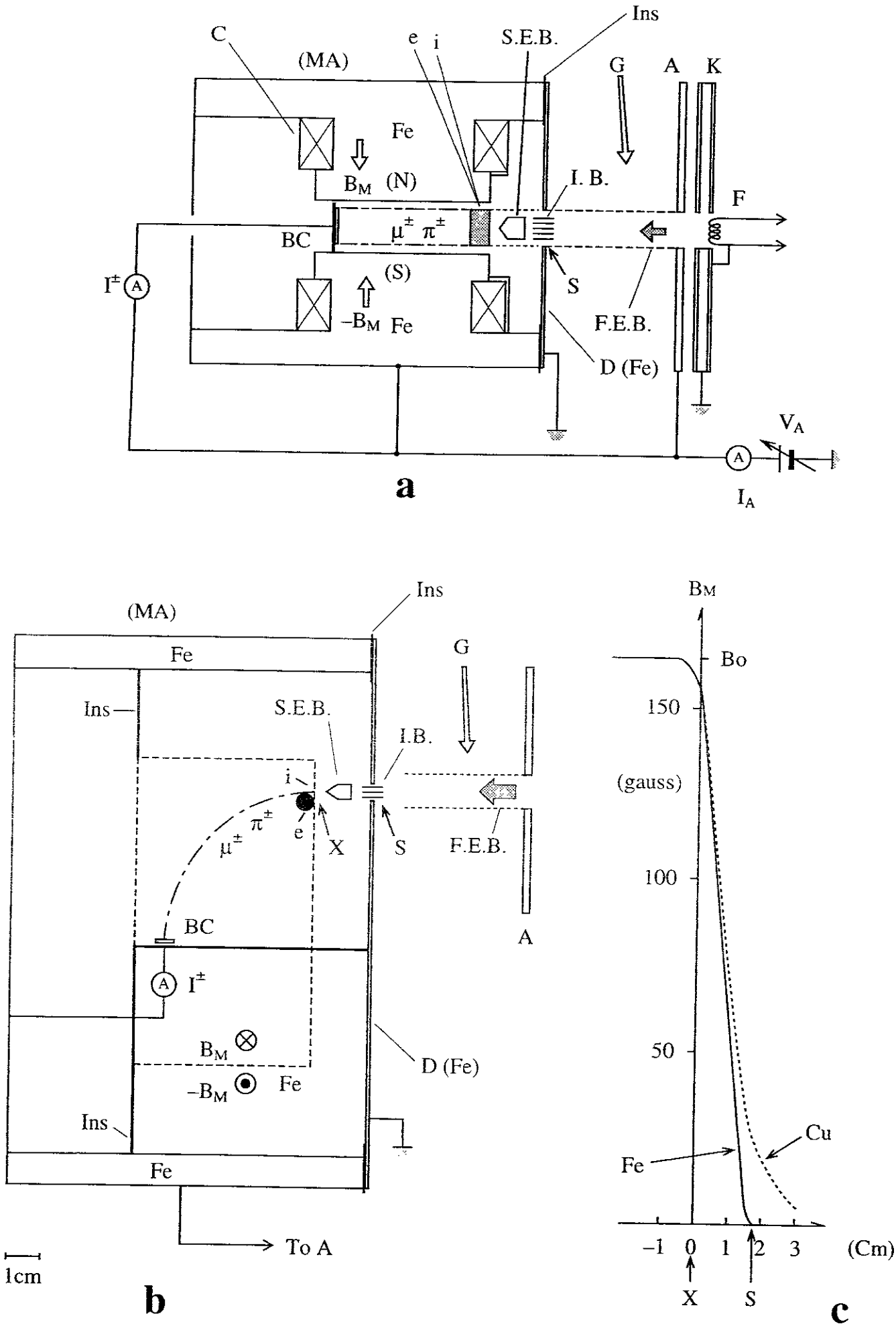
C
(MA)
e
i
S.E.B.
Ins
G
A
K
Fe
B_M (N)
I. B.
F
BC
$\mu^\pm$ $\pi^\pm$
(S)
$I^\pm$
$-B_M$ Fe
S
F.E.B.
D (Fe)
V_A
I_A
a
Ins
(MA)
Fe
G
Ins
S.E.B.
I.B.
i
$\pi^\pm$
$\mu^\pm$
e
X
S
F.E.B.
A
BC
$I^\pm$
B_M
$-B_M$ Fe
D (Fe)
Ins
Fe
To A
1cm
b
B_M
Bo
150
(gauss)
100
50
Cu
Fe
−1
0
1
2
3
(Cm)
X
S
c

Fig. 1

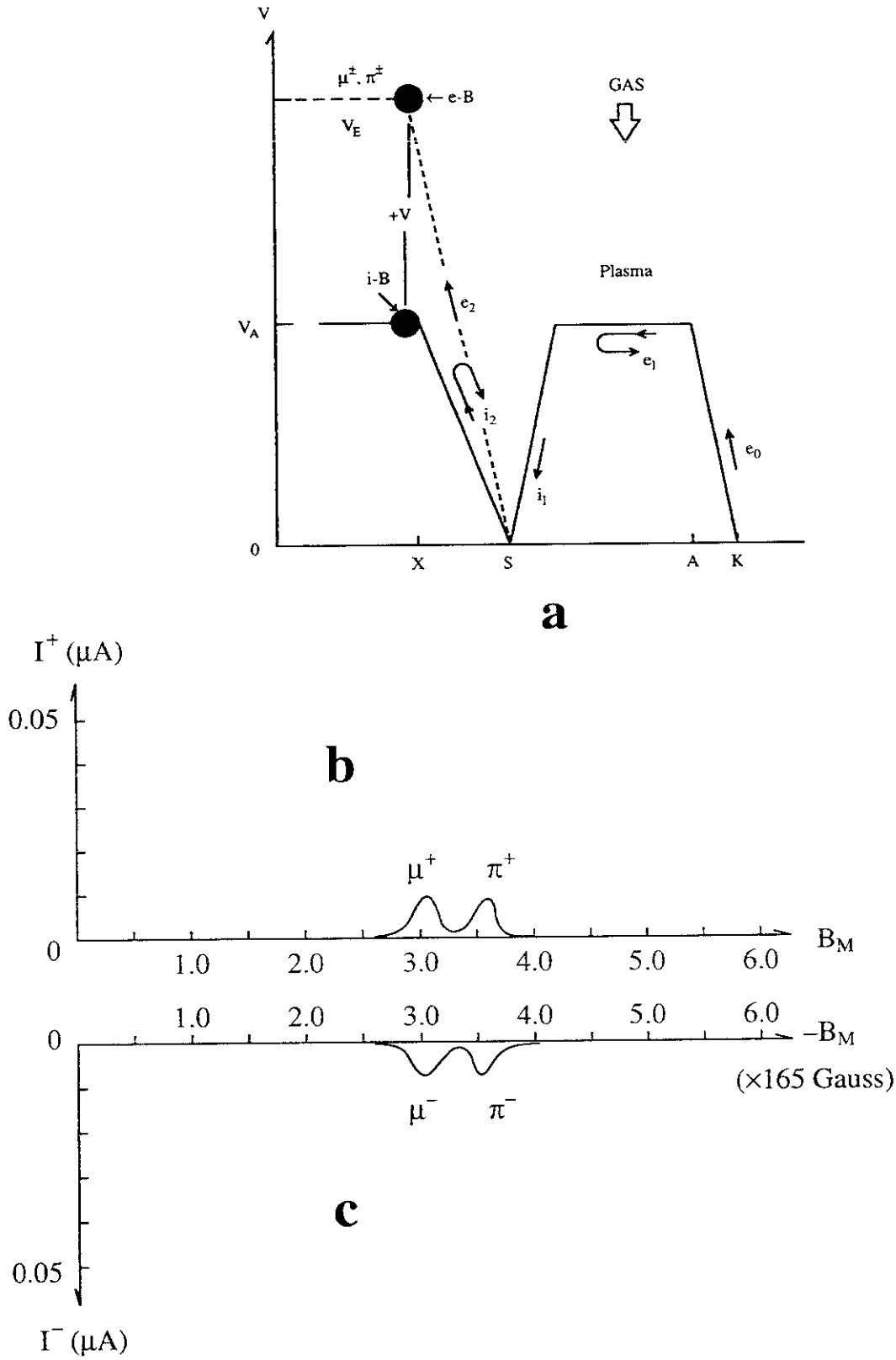
V
μ±, π±
← e-B
GAS
VE
+V
Plasma
i-B
e2
VA
e1
i2
e0
i1
0
X
S
A
K
a
I+ (μA)
0.05
b
μ+
π+
0
1.0
2.0
3.0
4.0
5.0
6.0
BM
1.0
2.0
3.0
4.0
5.0
6.0
0
−BM
(×165 Gauss)
μ−
π−
c
0.05
I− (μA)

Fig. 2

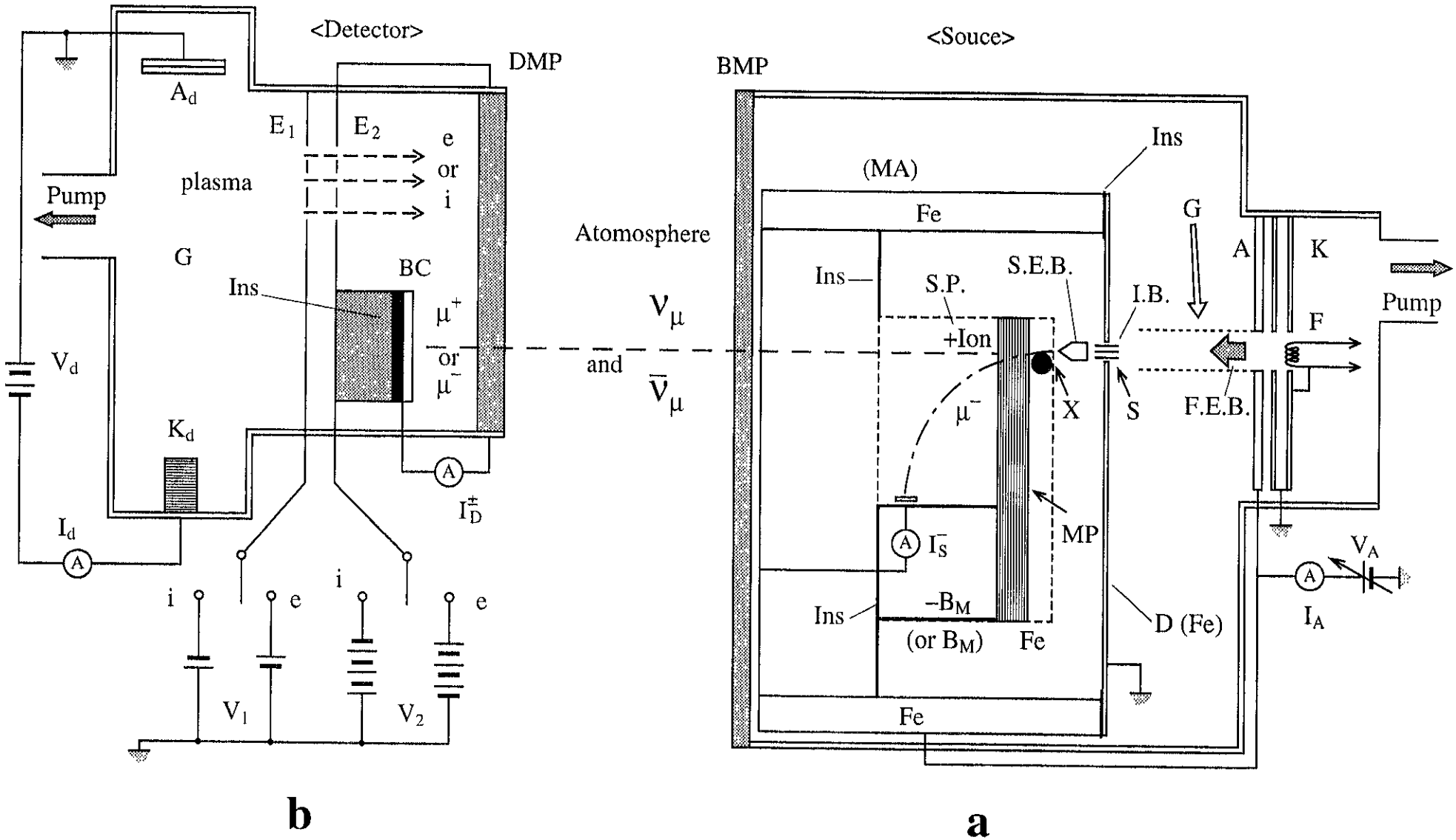
<Detector>
DMP
A_d
E_1
E_2
e
or
i
plasma
Pump
G
Ins
BC
μ^+
or
μ^-
V_d
K_d
I_d
$I_D^{\pm}$
i
e
i
e
V_1
V_2
Atomosphere
ν_μ
and
$\bar{\nu}_\mu$
<Souce>
BMP
(MA)
Ins
Fe
G
A
K
Ins
S.P.
S.E.B.
I.B.
Pump
F
+Ion
μ^-
X
S
F.E.B.
MP
I_S^-
V_A
I_A
Ins
$-B_M$
(or B_M)
Fe
D (Fe)
Fe

b **a**

Fig. 3

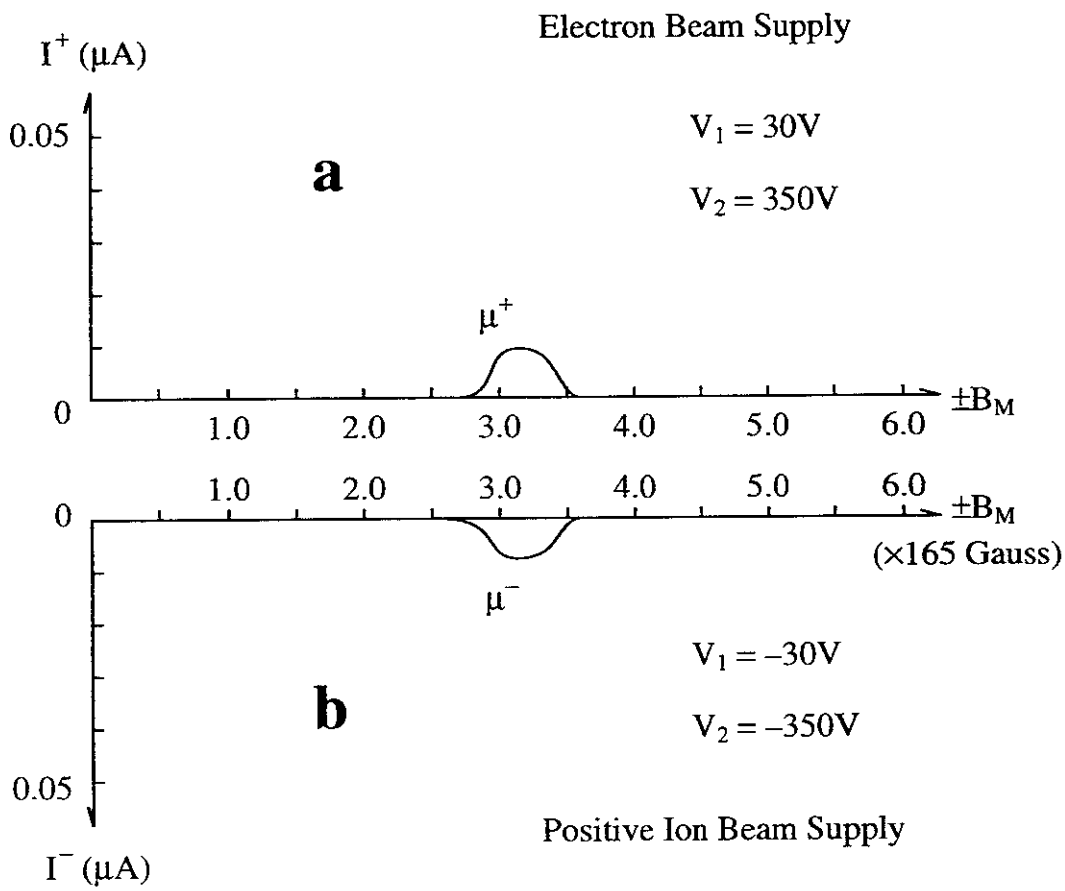
Electron Beam Supply
I^+ (μA)
0.05
a
$V_1 = 30V$
$V_2 = 350V$
μ^+
0
1.0
2.0
3.0
4.0
5.0
6.0
$\pm B_M$
1.0
2.0
3.0
4.0
5.0
6.0
0
$\pm B_M$
(×165 Gauss)
μ^-
$V_1 = -30V$
b
$V_2 = -350V$
0.05
Positive Ion Beam Supply
I^- (μA)

Fig. 4

Appendix

An experimental verification of metal plate penetration for the μ-neutrinos ν_μ and $\bar{\nu}_\mu$ can be done only inside the magnetic mass analyzer MA as shown in Figs. 1. Then, the positive pion π^+ beam is convenient as the penetration phenomenon appears more clearly in comparison with the negative pion π^- beam.

The first experimental arrangement without metal plate inside MA is shown in Figs. A1 **a** and **b** while a dependence of the positive current I^+ to BC on the analysis magnetic field B_M is shown in Fig. A1 **c**. Next, the second experimental arrangement with a thick (1 mm) metal plate MP inside MA is shown in Figs. A2 **a** and **b** where a distance between the MP and the BC is 2.0 cm. A dependence of the "negative" current I^- to BC on B_M is shown in Fig. A2 **c**. There, the positive pion π^+ beam seems to change into a negative muon μ^- beam from the curvature radius $r = 4.3$ cm of MA. That is, as the positive ions (+Ions) are supplied behind the MP from the secondary plasma S.P. around the analyzing magnetic field as shown in Fig. A2 **b**, the negative muon μ^- beam is generated by the μ-neutrino ν_μ beam due to the primary positive pion π^+ beam. If the distance between the MP and the BC is changed at 1 cm, the dependence of the I^- on B_M varys as shown in Fig. A3 **c** while we can consider two flights for π^+ and μ^- as shown in Fig. A3 **b**.

Finally, when the negative pion π^- beam is shot into the MP under the reversed analysis magnetic field ($-B_M$), the I^- current peak positions of π^- or μ^- for ($-B_M$) do not depend on the distance $\overline{MP - BC}$ and the MP itself as shown in Figs. A4 **a** and **b**.

Figure captions of Appendix

Figs. A1 **a** and **b** Schematic diagrams of the first experimental apparatus.

π^+: Positive pion beam. μ^+: Positive muon beam. B_M: Analysis magnetic field for positive particles. S.P.: Secondary plasma (around B_M) produced by I.B. and S.E.B..

(See captions of Figs. 1).

Fig. A1 **c** Dependence of positive current I^+ to BC on B_M.

π^+: Peak of I^+ corresponding to positive pion. μ^+: Peak of I^+ corresponding to positive muon.

Figs. A2 **a** and **b** Schematic diagrams of the second experimental apparatus.

π^+: Primary positive pion beam. MP: Metal plate (1 mm) shot by positive pion π^+ beam. $\overline{\text{MP} - \text{BC}}$: 2.0 cm. μ^-: Negative muon μ^- beam which generates from MP secondarily. I^-: Negative current to BC.

(See captions of Figs. 1 and Figs. A1).

Fig. A2 **c** Dependence of "negative" current I^- to BC on B_M.

μ^-: Peak of I^- corresponding to negative muon.

Figs. A3 **a** and **b** Schematic diagram of the third experimental apparatus and Dependence of "negative" current I^- to BC on B_M.

$\overline{\text{MP} - \text{BC}}$: 1.0 cm.

Figs. A4 **a** and **b** Schematic diagrams of the final experimental apparatus.

π^- or μ^-: Primary negative pion or muon beam. MP: Metal plate (1 mm) shot by negative pion π^- beam. $\overline{\text{MP} - \text{BC}}$: 2.0 cm. $(-B_M)$: Reversed analysis magnetic field. (μ^-) or (π^-): Secondary negative muon or pion beam which generates from MP.

(See captions of Figs. 1).

Fig. A4 **c** Dependence of negative current I^- to BC on $(-B_M)$.

(μ^-): Peak of I^- corresponding to secondary negative muon. (π^-): Peak of I^- corresponding to secondary negative pion.

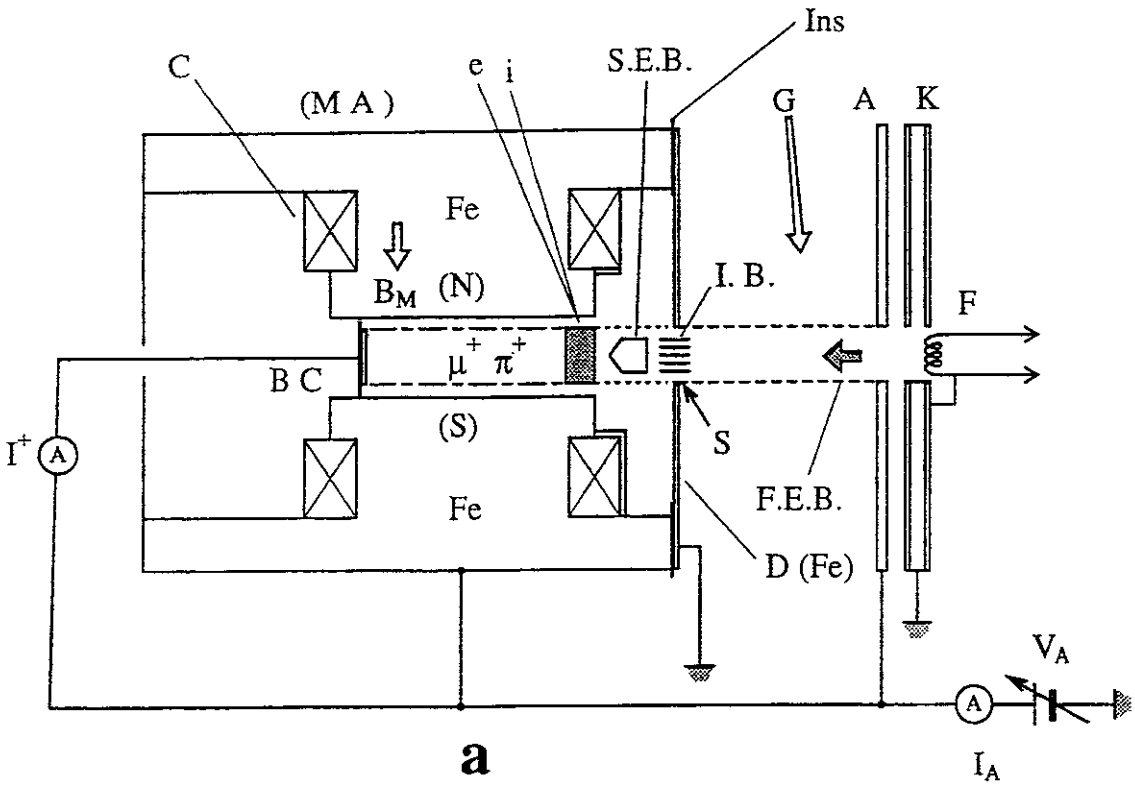
Ins
C
e
i
S.E.B.
(M A)
G
A
K
Fe
B_M
(N)
I. B.
F
μ^+ π^+
B C
(S)
S
I^+
A
Fe
F.E.B.
D (Fe)
V_A
A
I_A

a

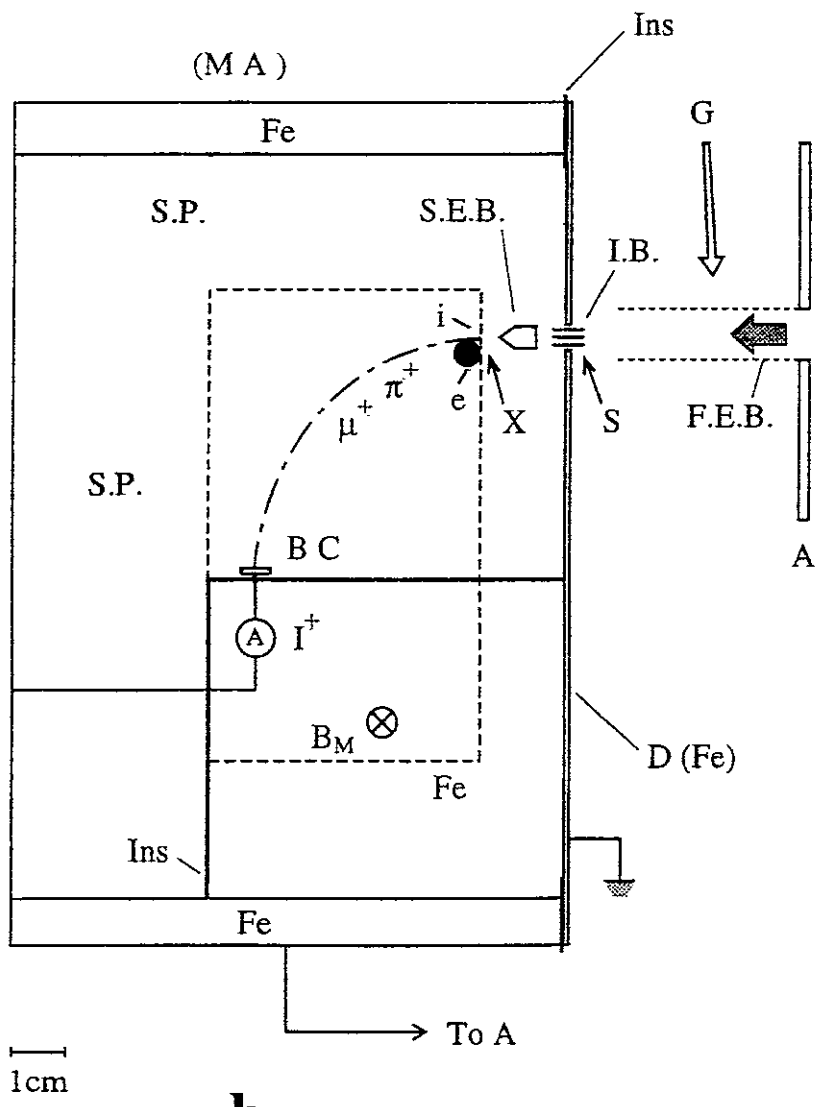
Ins
(M A)
Fe
G
S.P.
S.E.B.
I.B.
i
π^+
μ^+
e
X
S
F.E.B.
S.P.
A
B C
A
I^+
B_M
D (Fe)
Fe
Ins
Fe
To A
1cm

b

Fig. A1

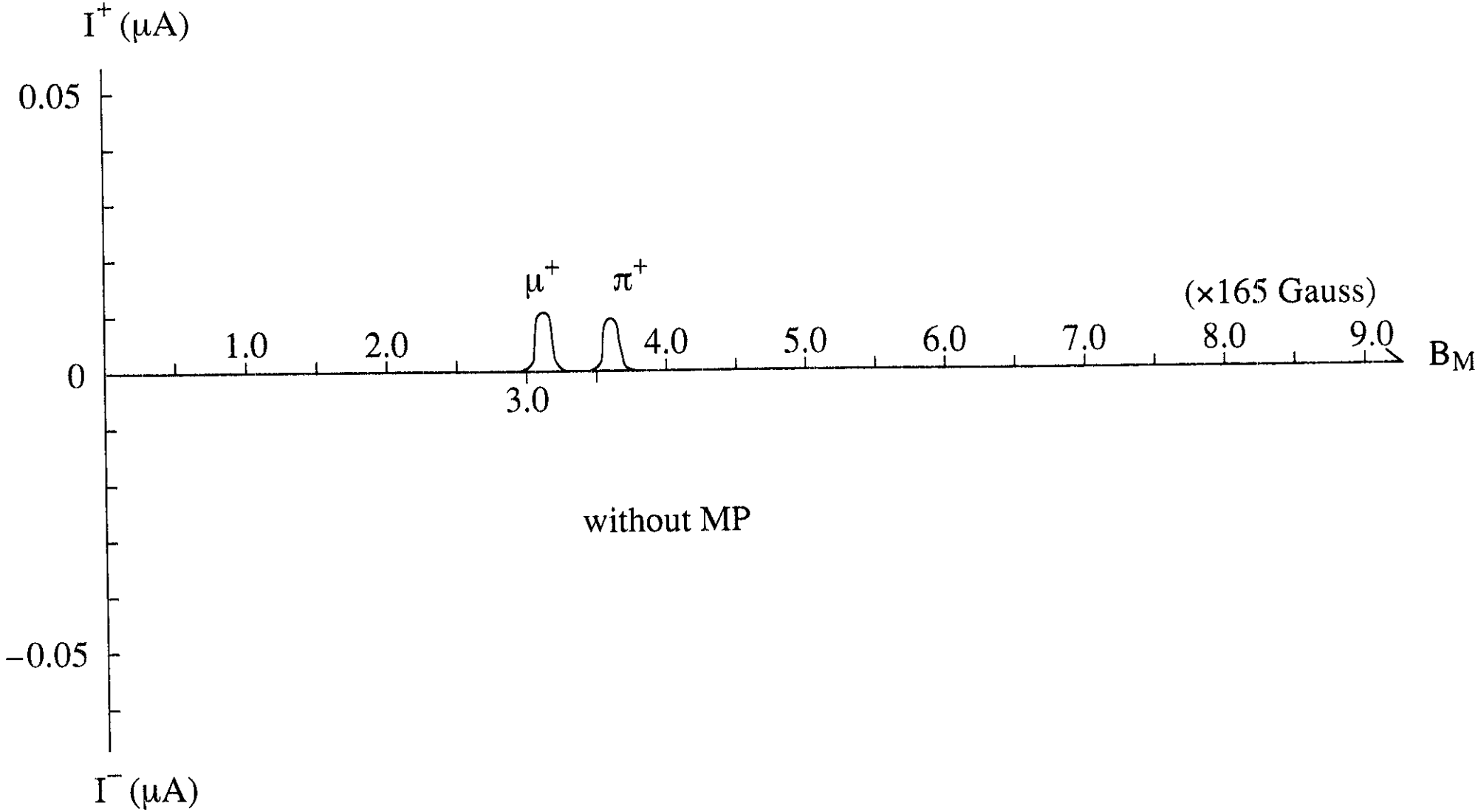
I+ (μA)
0.05
0
−0.05
I− (μA)
μ+
π+
(×165 Gauss)
1.0
2.0
3.0
4.0
5.0
6.0
7.0
8.0
9.0
BM
without MP

Fig. A1 **c**

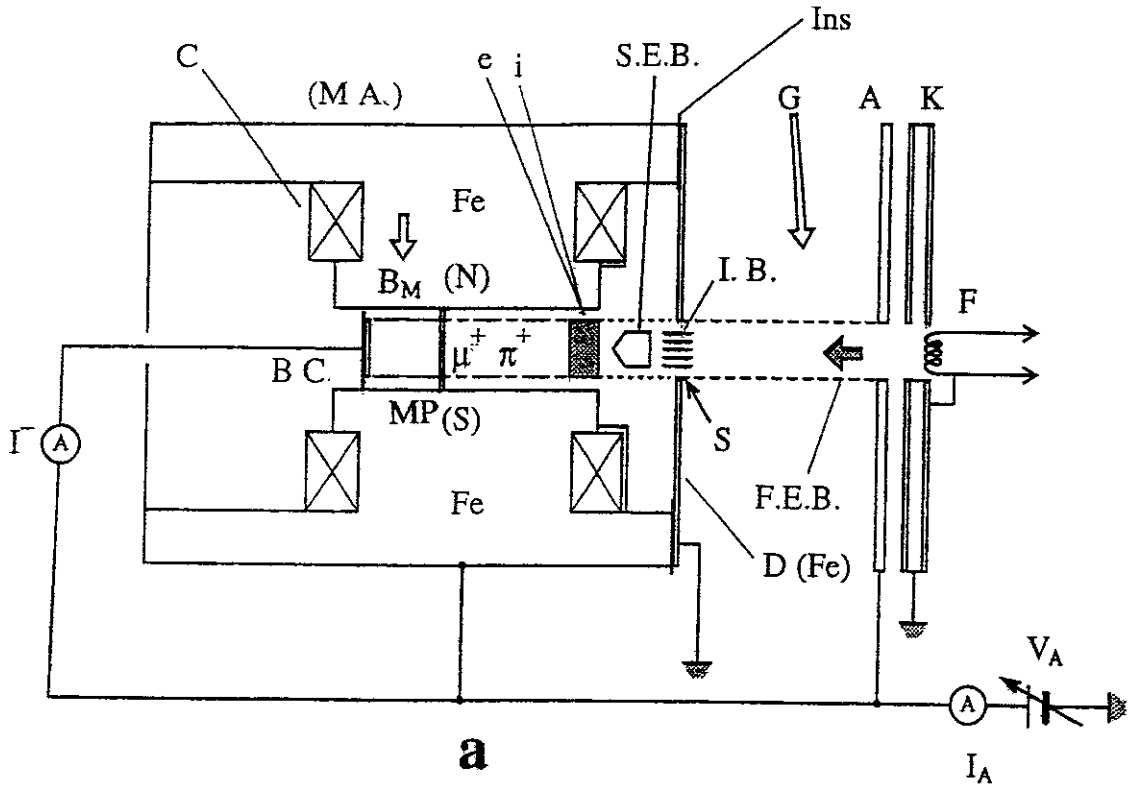
C
(M A.)
e
i
S.E.B.
Ins
G
A
K
Fe
B_M (N)
I. B.
F
μ^+ π^+
B C.
MP (S)
S
F.E.B.
Fe
D (Fe)
V_A
I_A

a

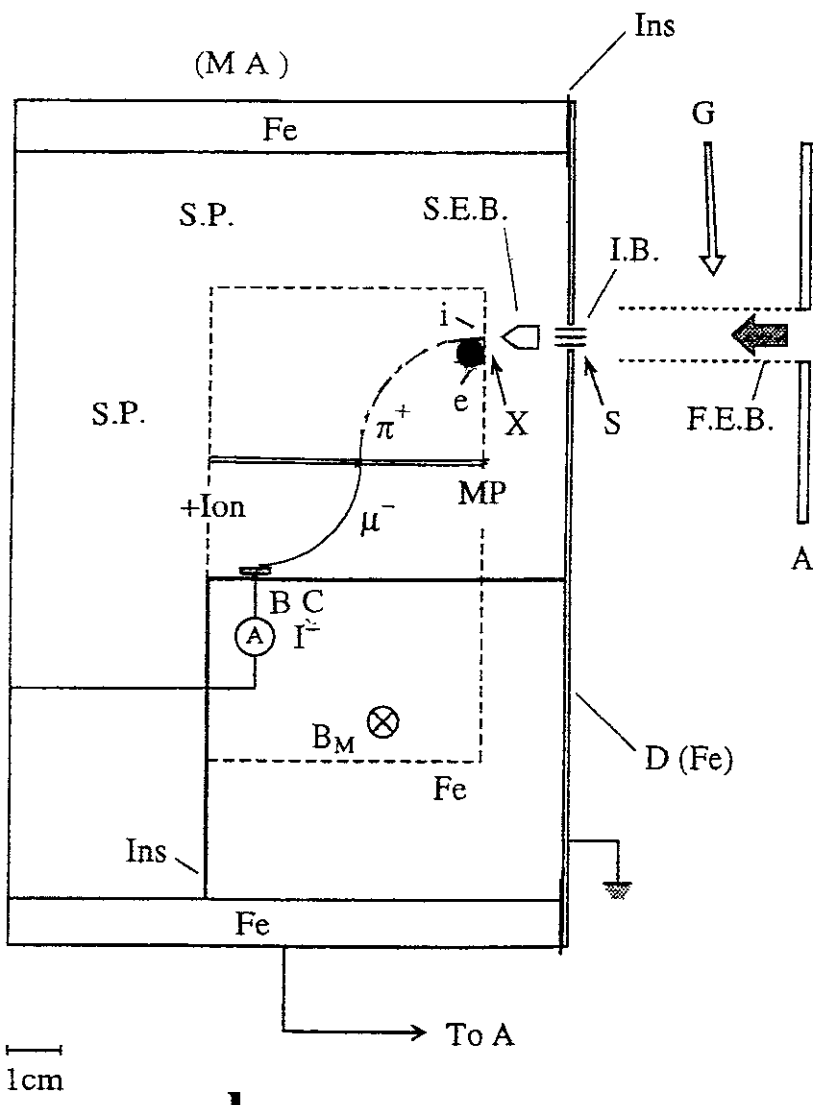
(M A)
Ins
Fe
G
S.P.
S.E.B.
I.B.
i
e
X
S
F.E.B.
S.P.
π^+
MP
+Ion
μ^-
A
B C
B_M
D (Fe)
Fe
Ins
Fe
To A
1cm

b

Fig. A2

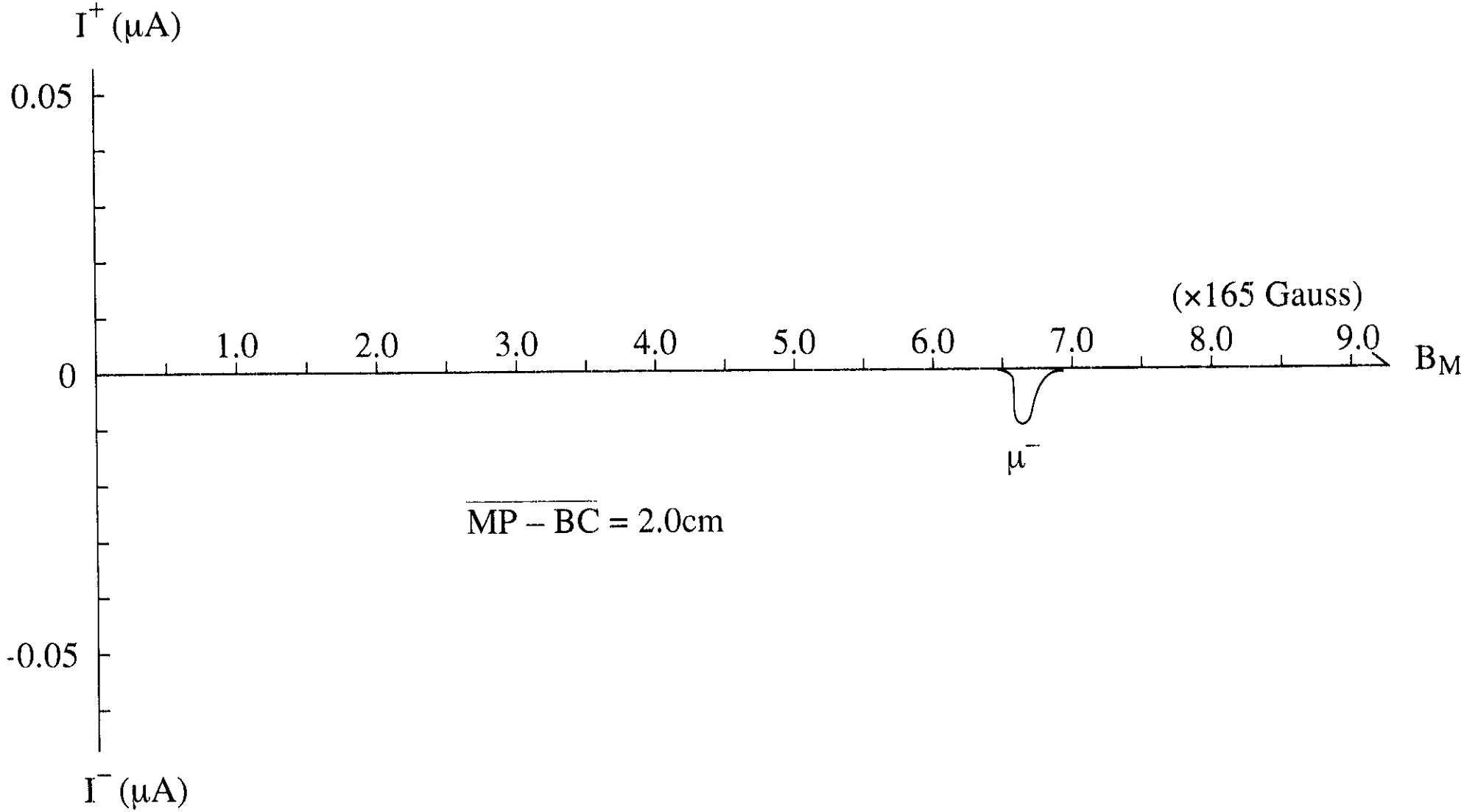
I+ (μA)
0.05
0
-0.05
I− (μA)
(×165 Gauss)
1.0
2.0
3.0
4.0
5.0
6.0
7.0
8.0
9.0
BM
μ−
MP – BC = 2.0cm

Fig. A2 **c**

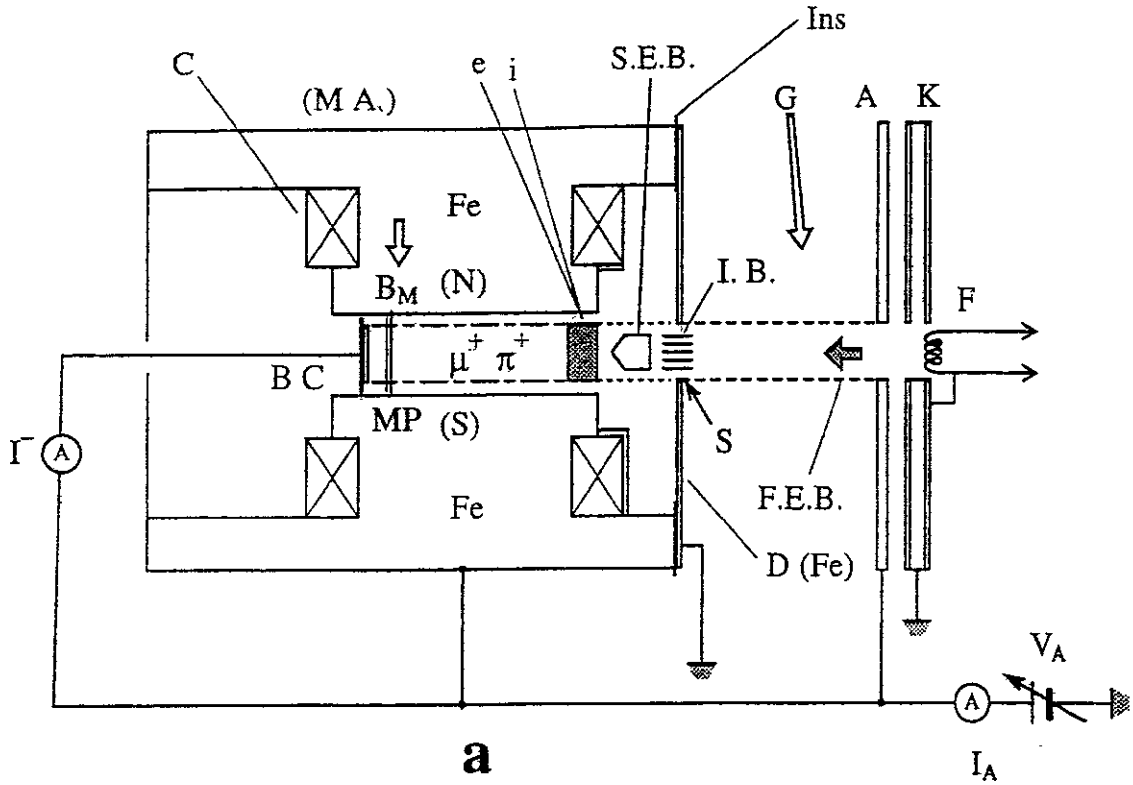
Ins
C
e
i
S.E.B.
(M A.)
G
A
K
Fe
B_M
(N)
I. B.
F
μ^+ π^+
B C
MP
(S)
S
F.E.B.
Fe
D (Fe)
V_A
I_A

a

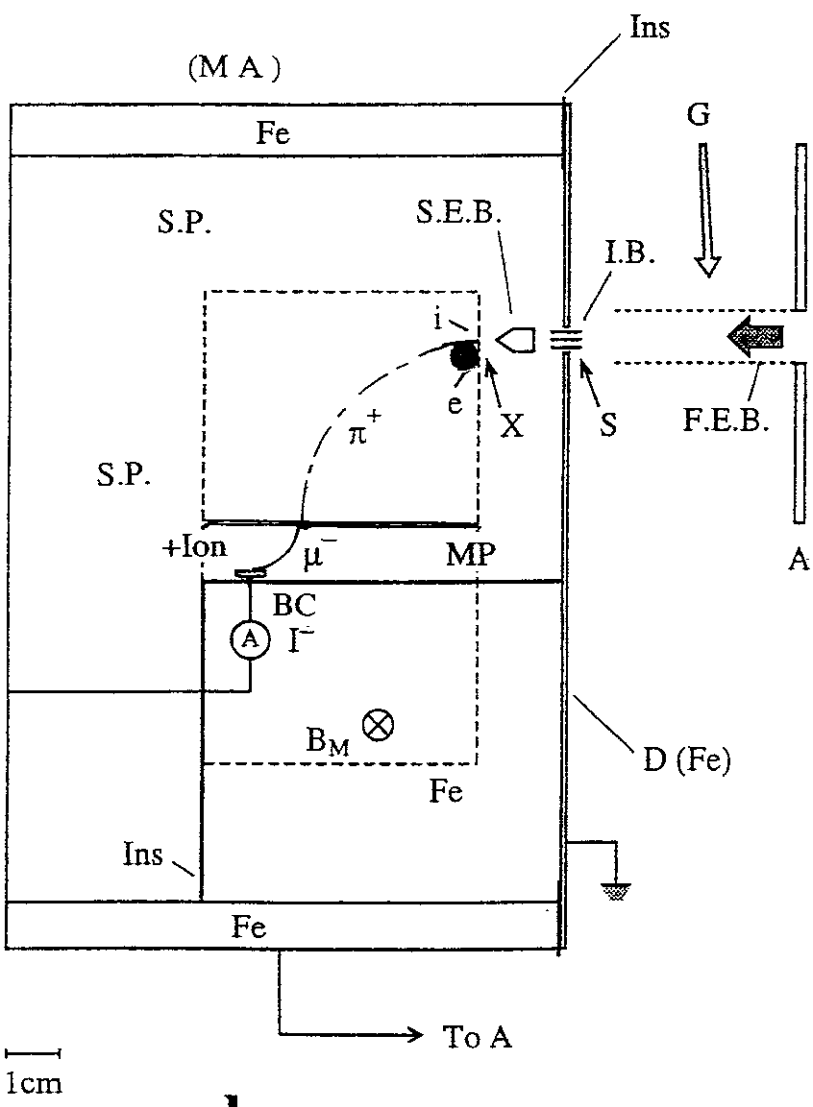
Ins
(M A)
G
Fe
S.P.
S.E.B.
I.B.
i
e
X
S
F.E.B.
π^+
S.P.
+Ion
μ^-
MP
A
BC
I^-
B_M
D (Fe)
Fe
Ins
Fe
To A
1cm

b

Fig. A3

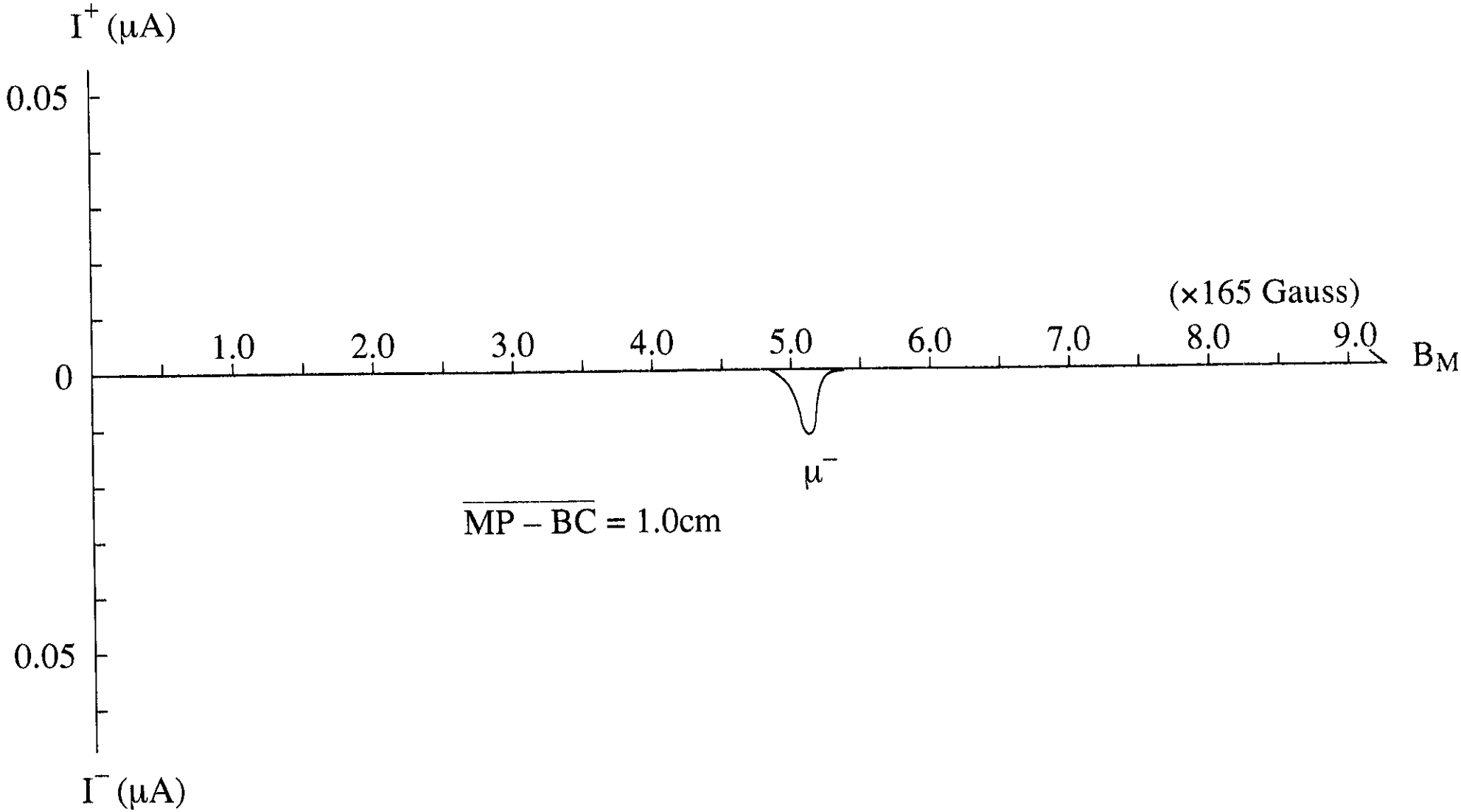
I+ (μA)
0.05
0
0.05
I− (μA)
1.0
2.0
3.0
4.0
5.0
6.0
7.0
8.0
9.0
(×165 Gauss)
BM
μ−
MP – BC = 1.0cm

Fig. A3 **c**

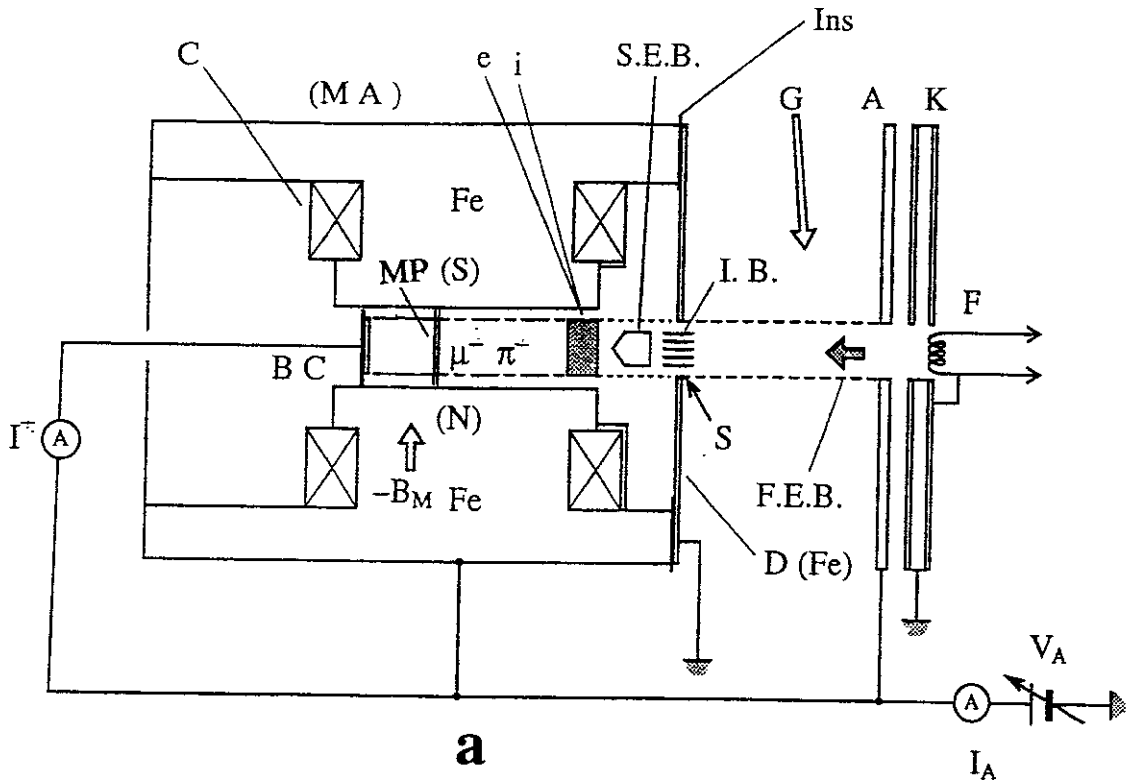
C
(M A)
e
i
S.E.B.
Ins
G
A
K
Fe
MP (S)
I. B.
F
B C
μ⁻ π⁻
(N)
S
F.E.B.
−B_M Fe
D (Fe)
V_A
I_A

a

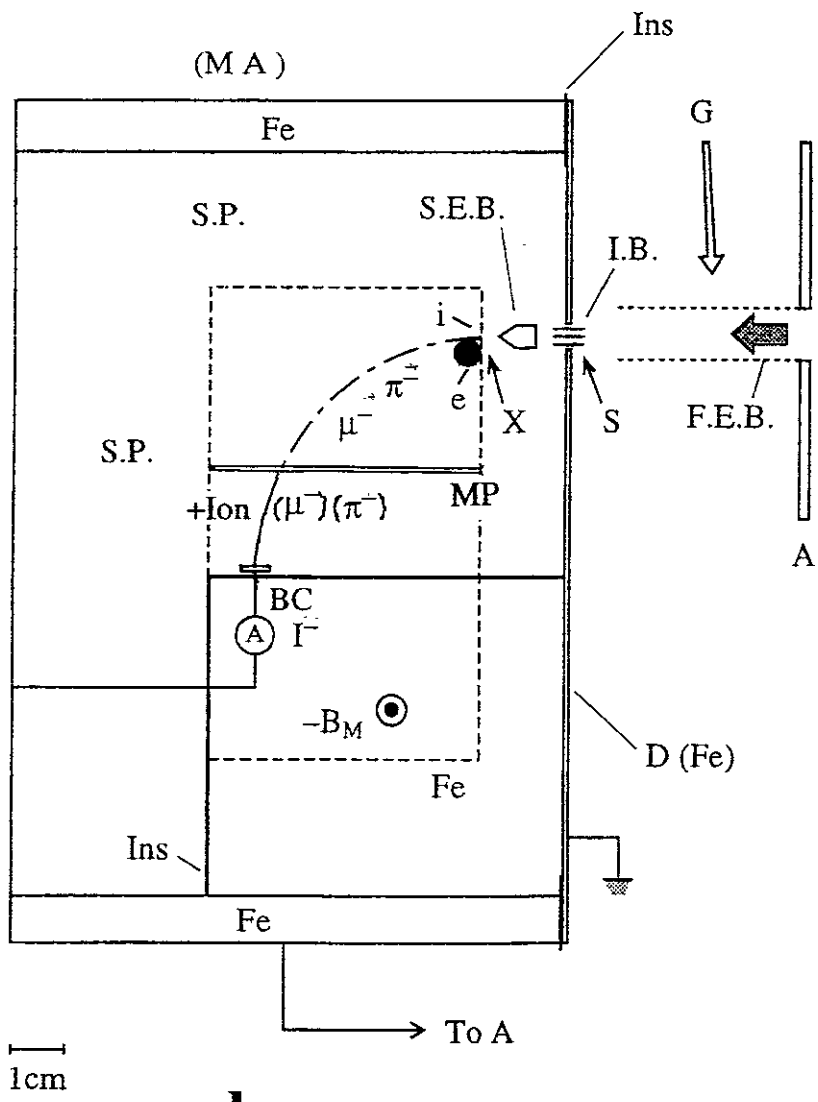
Ins
(M A)
Fe
G
S.P.
S.E.B.
I.B.
i
π⁻
e
X
μ⁻
S
F.E.B.
S.P.
+Ion (μ⁻)(π⁻)
MP
A
BC
I⁻
−B_M
D (Fe)
Fe
Ins
Fe
To A
1cm

b

Fig. A4

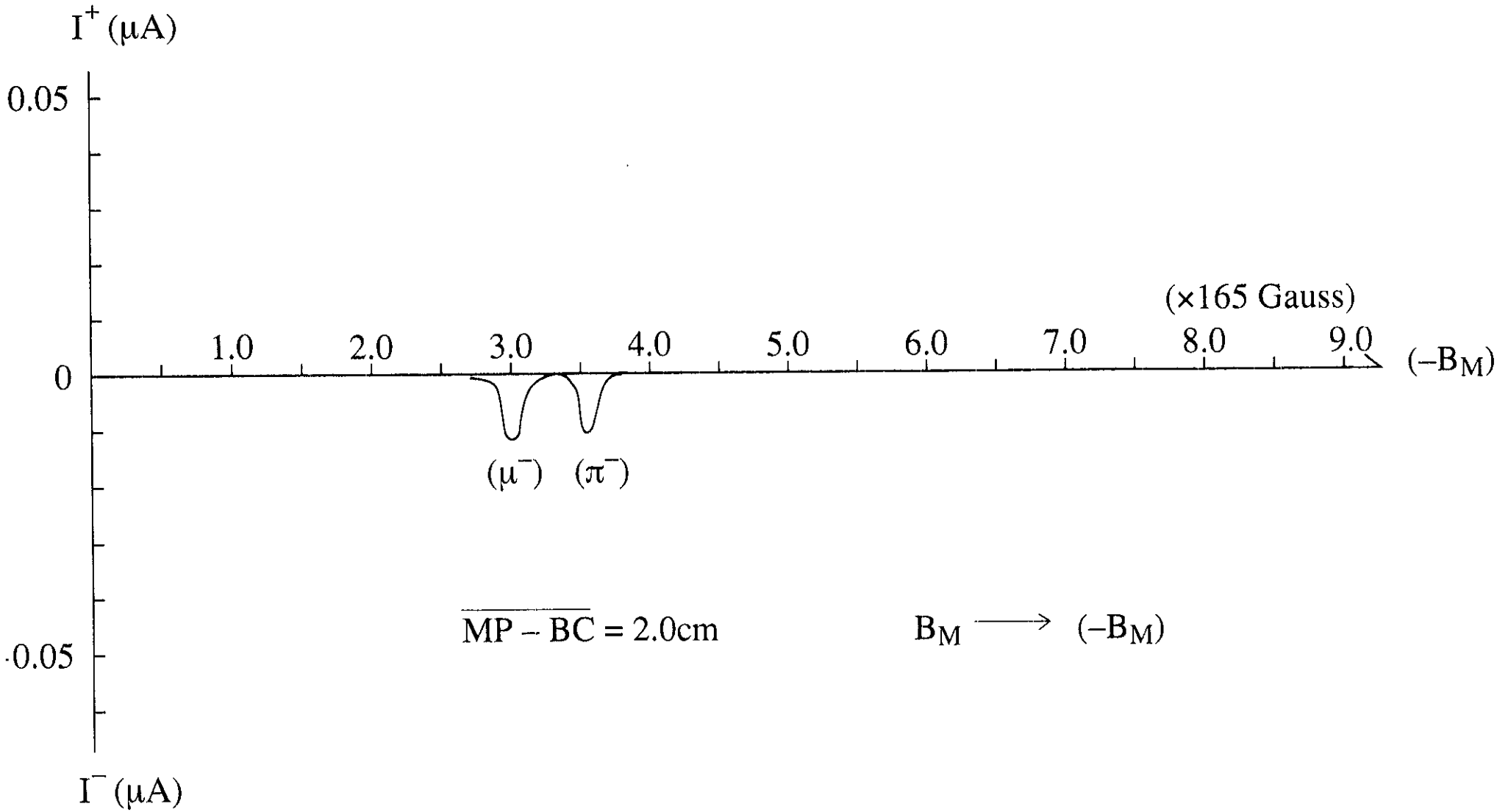
I+ (μA)
0.05
0
-0.05
I− (μA)
(×165 Gauss)
1.0
2.0
3.0
4.0
5.0
6.0
7.0
8.0
9.0
(−B_M)
(μ−)
(π−)
MP − BC = 2.0cm
B_M ⟶ (−B_M)

Fig. A4 **c**

Recent Issues of NIFS Series

NIFS-508 Y.-N. Nejoh,
Dynamics of the Dust Charging on Electrostatic Waves in a Dusty Plasma with Trapped Electrons; Sep.1997

NIFS-509 E. Matsunaga, T.Yabe and M. Tajima,
Baroclinic Vortex Generation by a Comet Shoemaker-Levy 9 Impact; Sep. 1997

NIFS-510 C.C. Hegna and N. Nakajima,
On the Stability of Mercier and Ballooning Modes in Stellarator Configurations; Oct. 1997

NIFS-511 K. Orito and T. Hatori,
Rotation and Oscillation of Nonlinear Dipole Vortex in the Drift-Unstable Plasma; Oct. 1997

NIFS-512 J. Uramoto,
Clear Detection of Negative Pionlike Particles from H_2 Gas Discharge in Magnetic Field; Oct. 1997

NIFS-513 T. Shimozuma, M. Sato, Y. Takita, S. Ito, S. Kubo, H. Idei, K. Ohkubo, T. Watari, T.S. Chu, K. Felch, P. Cahalan and C.M. Loring, Jr,
The First Preliminary Experiments on an 84 GHz Gyrotron with a Single-Stage Depressed Collector; Oct. 1997

NIFS-514 T. Shjmozuma, S. Morimoto, M. Sato, Y. Takita, S. Ito, S. Kubo, H. Idei, K. Ohkubo and T. Watari,
A Forced Gas-Cooled Single-Disk Window Using Silicon Nitride Composite for High Power CW Millimeter Waves; Oct. 1997

NIFS-515 K. Akaishi,
On the Solution of the Outgassing Equation for the Pump-down of an Unbaked Vacuum System; Oct. 1997

NIFS-516 *Papers Presented at the 6th H-mode Workshop (Seeon, Germany)*; Oct. 1997

NIFS-517 John L. Johnson,
The Quest for Fusion Energy; Oct. 1997

NIFS-518 J. Chen, N. Nakajima and M. Okamoto,
Shift-and-Inverse Lanczos Algorithm for Ideal MHD Stability Analysis; Nov. 1997

NIFS-519 M. Yokoyama, N. Nakajima and M. Okamoto,
Nonlinear Incompressible Poloidal Viscosity in L=2 Heliotron and Quasi-Symmetric Stellarators; Nov. 1997

NIFS-520 S. Kida and H. Miura,
Identificaiton and Analysis of Vortical Structures; Nov. 1997

NIFS-521 K. Ida, S. Nishimura, T. Minami, K. Tanaka, S. Okamura, M. Osakabe, H. Idei, S. Kubo, C. Takahashi and K. Matsuoka,
High Ion Temperature Mode in CHS Heliotron/torsatron Plasmas; Nov. 1997

NIFS-522 M. Yokoyama, N. Nakajima and M. Okamoto,
Realization and Classification of Symmetric Stellarator Configurations through Plasma Boundary Modulations; Dec. 1997

NIFS-523 H. Kitauchi,
Topological Structure of Magnetic Flux Lines Generated by Thermal Convection in a Rotating Spherical Shell; Dec. 1997

NIFS-524 T. Ohkawa,
Tunneling Electron Trap; Dec. 1997

NIFS-525 K. Itoh, S.-I. Itoh, M. Yagi, A. Fukuyama,
Solitary Radial Electric Field Structure in Tokamak Plasmas; Dec. 1997

NIFS-526 Andrey N. Lyakhov,
Alfven Instabilities in FRC Plasma; Dec. 1997

NIFS-527 J. Uramoto,
Net Current Increment of negative Muonlike Particle Produced by the Electron and Positiitve Ion Bunch-method; Dec. 1997

NIFS-528 Andrey N. Lyakhov,
Comments on Electrostastic Drift Instabilities in Field Reversed Configuraiton; Dec. 1997

NIFS-529 J. Uramoto,
Pair Creation of Negative and Positive Pionlike (Muonlike) Particle by Interaction between an Electron Bunch and a Positive Ion Bunch; Dec. 1997

NIFS-530 J. Uramoto,
Measuring Method of Decay Time of Negative Muonlike Particle by Beam Collector Applied RF Bias Voltage; Dec. 1997

NIFS-531 J. Uramoto,
Confirmation Method for Metal Plate Penetration of Low Energy Negative Pionlike or Muonlike Particle Beam under Positive Ions; Dec. 1997

NIFS-532 J. Uramoto,
Pair Creations of Negative and Positive Pionlike (Muonlike) Particle or K Mesonlike (Muonlike) Particle in H2 or D2 Gas Discharge in Magnetic Field; Dec. 1997

NIFS-533 S. Kawata, C. Boonmee, T. Teramoto, L. Drska, J. Limpouch, R. Liska, M. Sinor,
Computer-Assisted Particle-in-Cell Code Development; Dec. 1997

NIFS-534 Y. Matsukawa, T. Suda, S. Ohnuki and C. Namba,
Microstructure and Mechanical Property of Neutron Irradiated TiNi Shape Memory Alloy; Jan. 1998

NIFS-535 A. Fujisawa, H. Iguchi, H. Idei, S. Kubo, K. Matsuoka, S. Okamura, K. Tanaka, T. Minami, S. Ohdachi, S. Morita, H. Zushi, S. Lee, M. Osakabe, R. Akiyama, Y. Yoshimura, K. Toi, H. Sanuki, K. Itoh, A. Shimizu, S. Takagi, A. Ejiri, C. Takahashi, M. Kojima, S. Hidekuma, K. Ida, S. Nishimura, N. Inoue, R. Sakamoto, S.-I. Itoh, Y. Hamada, M. Fujiwara,
Discovery of Electric Pulsation in a Toroidal Helical Plasma; Jan. 1998

NIFS-536 Lj.R. Hadzievski, M.M. Skoric, M. Kono and T. Sato,
Simulation of Weak and Strong Langmuir Collapse Regimes; Jan. 1998

NIFS-537 H. Sugama, W. Horton,
Nonlinear Electromagnetic Gyrokinetic Equation for Plasmas with Large Mean Flows; Feb. 1998

NIFS-538 H. Iguchi, T.P. Crowley, A. Fujisawa, S. Lee, K. Tanaka, T. Minami, S. Nishimura, K. Ida, R. Akiyama, Y. Hamada, H., Idei. M. Isobe, M. Kojima, S. Kubo, S. Morita, S. Ohdachi, S. Okamura, M. Osakabe, K. Matsuoka, C. Takahashi and K. Toi,
Space Potential Fluctuations during MHD Activities in the Compact Helical System (CHS); Feb. 1998

NIFS-539 Takashi Yabe and Yan Zhang,
Effect of Ambient Gas on Three-Dimensional Breakup in Coronet Formation Process; Feb. 1998

NIFS-540 H. Nakamura, K. Ikeda and S. Yamaguchi,
Transport Coefficients of InSb in a Strong Magnetic Field; Feb. 1998

NIFS-541 J. Uramoto,
Development of ν_μ Beam Detector and Large Area ν_μ Beam Source by H_2 Gas Discharge (I); Mar. 1998

NIFS-542 J. Uramoto,
Development of $\bar{\nu}_\mu$ Beam Detector and Large Area $\bar{\nu}_\mu$ Beam Source by H_2 Gas Discharge (II); Mar. 1998

NIFS-543 J. Uramoto,
Some Problems inside a Mass Analyzer for Pions Extracted from a H_2 Gas Discharge; Mar. 1998

NIFS-544 J. Uramoto,
Simplified ν_μ $\bar{\nu}_\mu$ Beam Detector and ν_μ $\bar{\nu}_\mu$ Beam Source by Interaction between an Electron Bunch and a Positive Ion Bunch; Mar. 1998